이학석사 학위논문

크론병에서 조직 상주 기억 T 세포의 단일 세포 전사체 분석

Single-cell transcriptome analysis of tissue-resident memory T cells in Crohn's disease

울 산 대 학 교 대 학 원

의 과 학 과

이 윤 호

크론병에서 조직 상주 기억 T 세포의 단일 세포 전사체 분석

지 도 교 수 이 호 수

이 논문을 이학석사학위 논문으로 제출함

2024 년 2 월

울 산 대 학 교 대 학 원
의 과 학 과
이 윤 호

이윤호의 이학석사학위 논문을 인준함

심사위원 권 미 나 (인)

심사위원 한 범 (인)

심사위원 이 호 수 (인)

울 산 대 학 교 대 학 원

2024 년 2 월

ABSTRACT

Crohn's disease (CD) is a chronic inflammatory disorder affecting the bowel wall. Tissue-resident memory T (Trm) cells are implicated in CD, yet their characteristics remain unclear. We aimed to investigate the transcriptional profiles and functional characteristics of Trm cells in the small bowel of CD and their interactions with immune cells. Seven patients with CD and four with ulcerative colitis as controls were included. Single-cell RNA sequencing and paired T cell receptor sequencing assessed T cell subsets and transcriptional signatures in lamina propria (LP) and submucosa/muscularis propria-enriched fractions (SM/MP) from small bowel tissue samples. We identified 58,123 T cells grouped into 16 populations, including the Th17 Trm, $CD4^+$ Trm, and $CD8^+$ Trm clusters. In patients with CD, we identified Trm cells with a Th17 signature (termed Th17 Trm) in the bowel, demonstrating significantly increased proportions of the Th17 Trm cluster in both the LP and SM/MP areas. The Th17 Trm cluster demonstrated heightened expression of canonical tissue-residency marker genes (*ITGAE, ITGA1*, and *CXCR6*) along with elevated levels of *IL17A*, *IL22, CCR6,* and *CCL20*. The clonal expansion of Th17 Trm cells in CD was accompanied by enhanced transmural dynamic potential, as indicated by significantly higher migration scores. CD-prominent Th17 Trm cells displayed an increased interferon gamma (IFNγ)-related signature linked with *STAT1* activation, inducing chemokines (i.e., *CXCL10*, *CXCL8*, and *CXCL9*) in myeloid cells. Our findings underscored the elevated Th17 Trm cells throughout the small bowel in CD, contributing to disease pathogenesis through IFNγ induction and subsequent chemokine production in myeloid cells.

CONTENTS

LIST OF FIGURES

LIST OF TABLES

ABBREVIATIONS

CD	Crohn's disease
CM	Central memory
DE	Differential expression
DEG	Differentially expressed gene
FBS	Fetal bovine serum
IFNγ	Interferon gamma
LP	Lamina propria-enriched fraction
MT	Metallothionein
scRNA-seq	Single-cell RNA sequencing
scTCR-seq	Single-cell TCR sequencing
SM/MP	Submucosa/muscularis propria-enriched fraction
TCR	T cell receptor
Tem	Effector memory T cell
Tfh	Follicular helper T cell
TF	Transcription factor
Treg	Regulatory T cell
Trm	Tissue-resident memory T cell
UC	Ulcerative colitis
UMAP	Uniform manifold approximation and projection
UMI	Unique molecular identifiers

1. INTRODUCTION

Crohn's disease (CD) is a chronic inflammatory disorder that affects all layers of the bowel wall, characterized by transmural and patchy inflammation with skip lesions. While the exact cause remains unclear, it is widely accepted that T cells play a pivotal role in the pathogenesis of CD, positioning them as a significant target for therapeutic interventions aimed at reducing gut inflammation by inhibiting T cell recruitment to the gut.[1] However, the presence of tissue-resident memory T (Trm) cells within the gut poses challenges to such therapies, as these cells establish local pro-inflammatory populations that are not influenced by trafficking inhibitors.

Trm cells serve as essential immune sentinels in the gut,[2,3] with demonstrated longevity in the intestinal mucosa independent of circulating T cells.[4] They contribute to sustaining chronic immune responses and local inflammation,[5,6] playing a significant role in CD pathogenesis.[1,3,7,8] Furthermore, their ability to migrate across bowel layers implies the potential for vertical cellular crosstalk,[9] thus potentially influencing the transmural characteristics of CD. Experimental evidence confirms the involvement of Trm cells in disease flares,[3,10] while their depletion has shown protective effects against experimental colitis.[3,10] However, their precise role in modulating the inflammatory response in CD, especially within different gut compartments, remains poorly understood.[1]

To address this gap in knowledge, we comprehensively profiled a single-cell transcriptional and T cell receptor (TCR) profile using immune cells isolated from the small bowel of patients with CD. Our objective was to characterize the distribution of Trm cells and identify their transcriptional profiles in the gut and to investigate their potential interactions with other immune cells. By assessing the clonal expansion of Trm cells and studying their migration properties, we aimed to gain insights into the dynamics of these cells within the gut microenvironment.

2. MATERIALS AND METHODS

2.1 Tissue collection and preparation

We recruited seven CD patients with small bowel involvement, while four patients with ulcerative colitis (UC) served as a control group, providing non-involved small bowel tissues for comparison (Table 1). Non-inflamed small intestine tissue specimens, suitable for Trm cell characterization, were collected from CD and UC surgical resections in ice-cold RPMI 1640 (Gibco, UK). J.L.L. and Y.S.Y. assessed and extracted the unaffected margins of the resected tissue samples.

The samples were then promptly transferred to the laboratory, and tissue dissociation processes were initiated. Initially, tissues were rinsed with ice cold 1× phosphate buffered saline, and the mesenteric fat and epithelial layer were mechanically removed. Given the transmural nature of CD, we meticulously isolated the lamina propria-enriched fraction (LP) and the submucosa/muscularis propria-enriched fraction (SM/MP). Curved iris scissors (AC 451/10, Nopa Instruments, Tuttlingen, Germany) were used with precision to dissect within the submucosal layer, following a technique similar to that used in endoscopic submucosal dissection. The dissected LP and SM/MP fractions were minced into small pieces (<1 mm in diameter) and placed in digestion medium (0.05% collagenase IV (Sigma-Aldrich, St. Louis, MO, USA), 0.01% DNase I (Roche, Basel, Swiss) and 10% fetal bovine serum [FBS] in RPMI 1640). Tissues were digested in an incubator at 37°C for 30 min followed by 40 min with 90 rpm agitation for each LP and SM/MP. Dissociated cells were filtered through a 70 μm cell strainer (Falcon, Durham, NC, USA) and washed with RPMI 1640 containing 2% FBS following centrifugation at 400 relative centrifugal force for 10 min. Cell pellets were suspended in RPMI 1640 containing 2% FBS and filtered through a 40 μm cell strainer followed by centrifugation at 400 relative centrifugal force for 10 min.

2.2 Isolation of immune cells

To assess the changes in the immune cell landscape, we processed all samples by isolating $CD3^+$ or $CD45^+$ cells using magnetic bead sorting (Table 1). The isolation process was carried out using either MACS microbeads (catalog #130-097-043, Miltenyi Biotec, Teterow, Germany) or EasySep Human Cell Isolation Kits (catalog #17851, catalog #100-0105, Stemcell Technologies, Vancouver, BC, Canada), following the respective manufacturer's protocols. After successful cell isolation, each fraction was subjected to analysis using single-cell RNA sequencing (scRNA-seq) and single-cell TCR sequencing (scTCR-seq).

Table 1. Clinical characteristics of patients with CD and UC

	Sex	Age at Dx	Location at Dx	Behavior at Dx	Duration (m)	Surgery	Cause	Tx within 3m of surgery	Smoking*	Sorted cells	Methods
CD1	M	21.89	ileocolonic	penetrating	0.95	ileocolic resection	intra-abdominal abscess	none	current	CD3+	MACS
CD2	F	19.33	ileocolonic	stricturing	92.34	ileocolic resection	stricture	infliximab	never	CD3+	MACS
CD3	M	24.03	ileum	penetrating	0.76	small bowel resection	intra-abdominal abscess	steroids	current	CD3+	MACS
CD4	F	25.52	ileum	penetrating	188.91	small bowel resection	intra-abdominal abscess	azathiprine	fomer	CD45+	MACS
CD5	M	21.96	ileocolonic	stricturing	159.87	subtotal colectomy	stricture	azathiprine	never	CD45+	EasySep
CD6	F	13.18	ileocolonic	NSNP	230.20	right hemicolectomy	intra-abdominal abscess	none	never	CD45+	EasySep
CD7	F	16.00	ileocolonic	NSNP	115.69	ileocolic resection	intra-abdominal abscess	ustekinmab, steroids	never	CD3+	EasySep
UC1	F	39.54	unkonwn	-	237.89	total proctocolectomy	colorectal cancer (pT1N0Mx)	vedolizumab	never	CD45+	MACS
UC2	F	12.11	unkonwn	-	390.46	total proctocolectomy	colorectal cancer (pT3N0Mx)	5-ASA	never	CD45+	EasySep
UC3	F	34.35	proctitis	-	54.31	total proctocolectomy	medically refractory colitis	infliximab, steroids, 5-ASA	never	CD45+	EasySep
UC4	F	18.82	unkonwn	-	180.36	total proctocolectomy	colorectal cancer (pT1N0Mx)	tofacitinib	never	CD3+	EasySep

*Smoking status at surgery

ASA, aminosalicylic acid; CD, Crohn's disease; Dx, diagnosis; NSNP, non-stricturing, non-penetrating; m, month; Tx, treatment; UC, ulcerative colitis.

2.3 Single cell RNA sequencing and TCR sequencing

Sorted $CD3^+$ cells or $CD45^+$ cells were resuspended in 1× phosphate buffered saline and filtered through a 40 μm filter. After cells were counted using LUNA-FL™ Automated Fluorescence Cell Counter, we utilized the 10x Genomics Chromium Instrument and cDNA synthesis kit (Chromium Next GEM Single Cell 5′ Kit v2 & Chromium Next GEM Chip K Single Cell Kit) to generate a barcoded cDNA library for single Cell RNA-sequencing. cDNA library quality was determined using an Agilent Bioanalyzer. Using this library, we ran two paired-end 200bp FlowCells on an Illumina NovaSeq6000 S2 Rgt Kit v1.5 [200 cycles (Read lengths: 28 bp Read1, 10 bp I7 Index, 10 bp I5 Index, and 90 bp Read2)].

For TCR Sequencing, we used cDNA to process a nested-PCR enrichment method to increase specificity of the amplification the constant region of the T-cell transcripts. Using 10X Genomics Chromium Single Cell Human TCR Amplification Kit, TCR libraries were enriched for Alpha-beta (TRA/B) TCRs. TCR library quality was determined using an Agilent Bioanalyzer. Using this library, we ran two paired-end 200bp FlowCells on an Illumina NovaSeq6000 S2 Rgt Kit v1.5 [200 cycles (Read lengths: 50 bp Read1, 10 bp I7 Index, 10 bp I5 Index, and 100 bp Read2)].

2.4 Single cell RNA sequencing data analysis

Following sequencing, binary base call files were demultiplexed using CellRanger v6.1.2.[11] Raw FASTQ files were aligned to the human GRCh38 reference genome, and unique molecular identifiers (UMI) counts were quantified using CellRanger v6.1.2. Filtered data matrices were employed for the subsequent analyses. To prevent biased clustering based on TCR gene expression patterns, gene expression counts for TCR genes were excluded. High-quality cells were selected based on the following criteria: 1) cells with >500 genes, 2) cells with <3500 genes, and 3) cells with <15% mitochondrial gene expression in the UMI counts. The identification and removal of doublets was performed using DoubletFinder v2.0.3.[12]

To mitigate batch effects in the datasets, we implemented the Seurat v4 integration workflow.[13] Initially, gene expression matrices from each sample were normalized to the total UMI counts per cell and logarithmically transformed. Subsequently, 2,000 highly variable genes were identified using the FindVariableFeatures function in Seurat with the vst method. Anchors, representing shared biological cell states, were detected across all samples, and integration was carried out utilizing these anchors. Furthermore, a cell cycle score was computed for each cell based on its expression of G2/M and S phase marker genes in the integrated data using the CellCycleScoring function in Seurat v4. These scores were then regressed out during data scaling via the ScaleData function in Seurat v4.

Principal component analysis was conducted on the top 2,000 highly variable genes, selected

as the variable genes. Uniform manifold approximation and projection (UMAP) were subsequently applied to the integrated object. For the final clustering step, the integrated object was clustered employing the first 20 principal components and a resolution of 0.5. For the subsequent removal of non-T cell clusters, we used global clustering to identify a total of $CD3D^+$ T cells. This process identified a total of 58,123 T cells, including 24,987 LP T cells and 33,136 SM/MP T cells, and the aforementioned integration workflow was reiterated using only these T cells. The sample with the highest cell count contained 6,359 cells, while the smallest sample consisted of 678 cells (Figure 1A). To ascertain the cell identities, marker genes for each cluster were determined using the FindAllMarkers function in Seurat v4.[13] Subsequently, cell type annotation was manually conducted based on established marker gene expression patterns for distinct cellular states (Table 2).

2.5 Differential expression analysis

Differential expression (DE) analysis in the scRNA-seq dataset was performed using the FindMarkers function in Seurat v4, employing the MAST method.[14] Only genes present in a minimum of 25% of cells within each cluster or group were included in the DE analysis. Differentially expressed genes (DEGs) were identified based on an adjusted p-value threshold of less than 0.05 and a log fold-change exceeding 0.5 in the average expression values, as determined through the DE analysis process. Gene Ontology pathway enrichment analysis was conducted utilizing the Clusterprofiler R package[15], and gene set enrichment analysis was conducted using the fgsea R package.[16] Pathways with a false discovery rate below 0.05 were considered as significant.

2.6 Gene regulatory network analysis

Transcription factor (TF) module activities within the scRNA-seq data were calculated using the single-cell regulatory network inference and clustering (SCENIC) package in R,[17] in conjunction with the RcisTarget database. Genes detected in less than 1% of total cells were filtered out. Additionally, a random sampling of 1,000 cells was performed for each cluster, and coexpression modules were identified using these cells based on the GENIE3 algorithm.[18] This process led to the discovery of TF modules, leveraging the expression profiles of 8,591 genes across approximately 14,000 T cells. Subsequently, activities for TF modules, comprised of both TF and target genes, were calculated across all cells, employing the AUCell function. The identification of TF modules specific to each cluster was accomplished using the calcRSS function within the SCENIC package.

2.7 TCR repertoire analysis

For TCR data analysis, TCR reads were aligned to the GRCh38 Cellranger VDJ reference

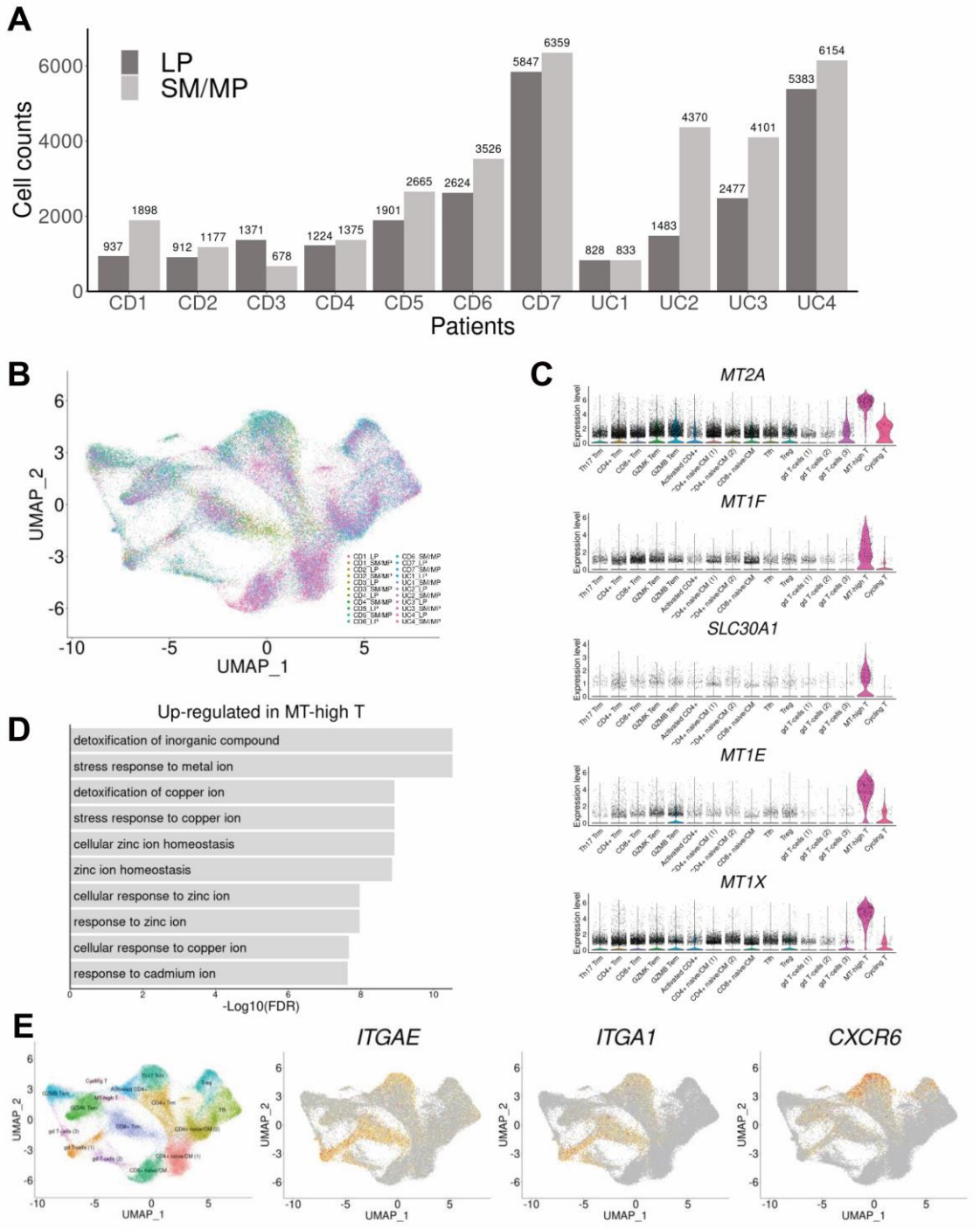

Figure 1. Cluster-specific single cell gene expression. (A) Bar plot showing the number of cells remaining in each sample after QC. (B) UMAP (Uniform manifold approximation and projection) plot of all sorted T cells visualized by each sample. (C) Violin plots showing the expression levels of top five differentially expressed genes in the differential expression analysis between the metallothionein (MT)-high T cluster and other clusters. (D) The result of GO pathway enrichment analysis for significantly up-regulated genes in MT-high T cluster. (E) Expression of canonical tissue-residency markers in $CD3^+$ T cells.

Table 2. Representative cell markers of 16 T cell clusters

T cell clusters		Marker genes
Th17 Trm	Tissue resident memory Th17 cells	*CD4, IL17A, IL22, CXCR6, CCL20, KLRB1, RORC, RORA, CCR6, IL23R, I*
$CD4^+$ Trm	$CD4^+$ Tissue resident memory T cells	*CD4, IL7R, ANXA1, LMNA, S100A11, VIM, TIMP1, ICOS*
$CD8^+$ Trm	$CD8^+$ Tissue resident memory T cells	*CD8A, CD8B, XCL1, CD160, ITGAE, ITGA1, KLRC1, SPRY1, RUNX3, CXC*
GZMK Tem	$CD8^+$ $GZMK^+$ effector memory T cells	*CD8A, CD8B, GZMK, IFNG, NKG7, GZMH, EOMES, GZMM, GZMA*
GZMB Tem	$CD8^+$ $GZMB^+$ effector memory T cells	*CD8A, CD8B, GZMB, FGFBP2, GZMH, GNLY, PRF1, IFNG, KLRD1, GZM*
Activated $CD4^+$	Activated $CD4^+$ T cells	*CD4, HLA-DRB1, HLA-DRA, TNF, HLA-DPA1, IFNG, HLA-DRB5, TGFB1,*
$CD4^+$ naïve/CM (1)	$CD4^+$ naïve/central memory T cells (1)	*CD4, SELL, CCR7, KLF2, LEF1, TCF7, S1PR1*
$CD4^+$ naïve/CM (2)	$CD4^+$ naïve/central memory T cells (2)	*CD4, CCR7, JUN, JUNB, FOS, TCF7, FOSB*
$CD8^+$ naïve/CM	$CD8^+$ naïve/central memory T cells	*CD8A, CD8B, SELL, CCR7, KLF2, LEF1, TCF7*
Tfh	$CD4^+$ follicular helper T cells	*CD4, CXCR5, CXCL13, TOX2*
Treg	$CD4^+$ regulatroy T cells	*CD4, FOXP3, CTLA4*
gd T-cells (1)	gamma delta T cells (1)	*TRDC, GNLY, GZMA, KIR2DL4, TYROBP, KLRC2, CD160, KLRD1*
gd T-cells (2)	gamma delta T cells (2)	*TRDC, TRDV1, KLRC2, CD160, TRGV4, KIR3DL2*
gd T-cells (3)	gamma delta T cells (3)	*TRDC, GNLY, TYROBP, GZMB, PRF1, KLRD1, GZMA*
MT-high T	Metallothionein-high T cells	*MT2A, MT1X, MT1E, MT1F, MT1G, SLC30A1*
Cycling T	Cycling T cells	*MKI67, TUBB*

genome (cellranger-vdj-GRCh38-alts-ensembl-7.1.0) for each sample using Cellranger vdj software. The resulting files encompassed CDR3 nucleotide sequences, CDR3 amino acid sequences, and V(D)J genes of alpha- or beta-chains for each individual cell. To enhance the robustness of our downstream analysis, we exclusively considered clonotypes comprising highly confident and productive chains. Additionally, for heightened accuracy, cells with more than one clonotype for the same chain type were excluded from the TCR analysis. A clonotype was defined as the same when cells exhibited identical V(D)J genes and CDR3 nucleotide sequences within samples from a specific patient.

Clonotypes were categorized as expanded if the count of cells sharing the same clonotypes within each sample exceeded two. Subsequently, for each sample, the expanded clonotypes were divided into four quantiles based on their frequencies, resulting in classification as 'High', 'Intermediate', or 'Low' groups. To provide insights into the nature of the TCR repertoire and its diversity within the studied samples, “Expansion scores” within clusters for each sample were calculated using the STARTRAC package v0.1.0.[19] We also used the STARTRAC package to calculate "Transition scores,” which represent state transitions of T cell clusters, and "Migration scores,” which indicate migration within paired samples from each patient. TCR diversity metrics, such as Shannon entropy, were assessed using the tcR package.[20]

2.8 Ligand-receptor interaction analysis

We employed the NicheNet R package to compute ligand-receptor interactions between Trm and other immune cells.[21] Firstly, we extracted ligands from the pool of ligand genes expressed in Trm, focusing solely on those available in the NicheNet database. Subsequently, by conducting DE analysis on myeloid cells from CD and UC patients, we generated a list of candidate target genes predicted to be influenced by ligand-receptor interactions. Lastly, we prioritized the ligands expressed in Trm using prediction scores for target genes expressed in myeloid cells.

3. RESULTS

3.1 Analyzing T cell diversity and distribution across gut niches

A combined total of 58,123 T cells, including 24,987 LP T cells and 33,136 SM/MP T cells (Figure 2A), were collectively clustered from the 22 samples. Utilizing UMAP for visualizing expression profiles, we identified 16 distinct clusters across all samples (Figure 2B-C). Annotation of these clusters based on marker genes revealed diverse T cell subsets (Figure 2D and Table 2). Particularly, a distinct metallothionein (MT)-high T cluster was observed within the SM/MP, exhibiting pronounced expression of metallothionein-associated genes, including *MT2A*, *MT1E*, *MT1F*, and *MT1X*, along with the *SLC30A1* associated with zinc ion transmembrane transporter activity (Figure 1). Notably, approximately 30% of the total cells were allocated to the three Trm clusters. The Th17 Trm and $CD8^+$ Trm clusters exhibited high expression levels of canonical tissue-residency markers, including *ITGAE* (CD103) and *ITGA1* (CD49a), with the addition of *CXCR6* primarily observed in the Th17 Trm cluster (Figure 1E). In contrast, the $CD4^+$ Trm cluster displayed lower expression of *ITGAE*, in line with previous studies emphasizing the differential expression of *ITGAE* between $CD8^+$ Trm and $CD4^+$ Trm clusters.[22-24] Furthermore, *CD69*, commonly employed as a marker of tissue retention, was found to be widely expressed among T cells in the gut.

Cell type proportions were assessed in each sample, revealing marked differences based on disease status (Figure 2C-E). Patients with CD exhibited significantly increased proportions of the Th17 Trm cluster in both the LP and SM/MP areas compared to patients with UC. Additionally, Patients with CD displayed heightened proportions of the activated $CD4^+$ cluster and gd T cells (2), particularly in the SM/MP area, while UC patients showed elevated proportions of the $CD4^+$ naïve/central memory (CM) (1) cluster and $CD8^+$ naïve/CM cluster at both locations. These findings collectively indicated notable quantitative shifts in T cell subtypes within the small bowel due to CD, consistently observed in both the LP and SM/MP regions.

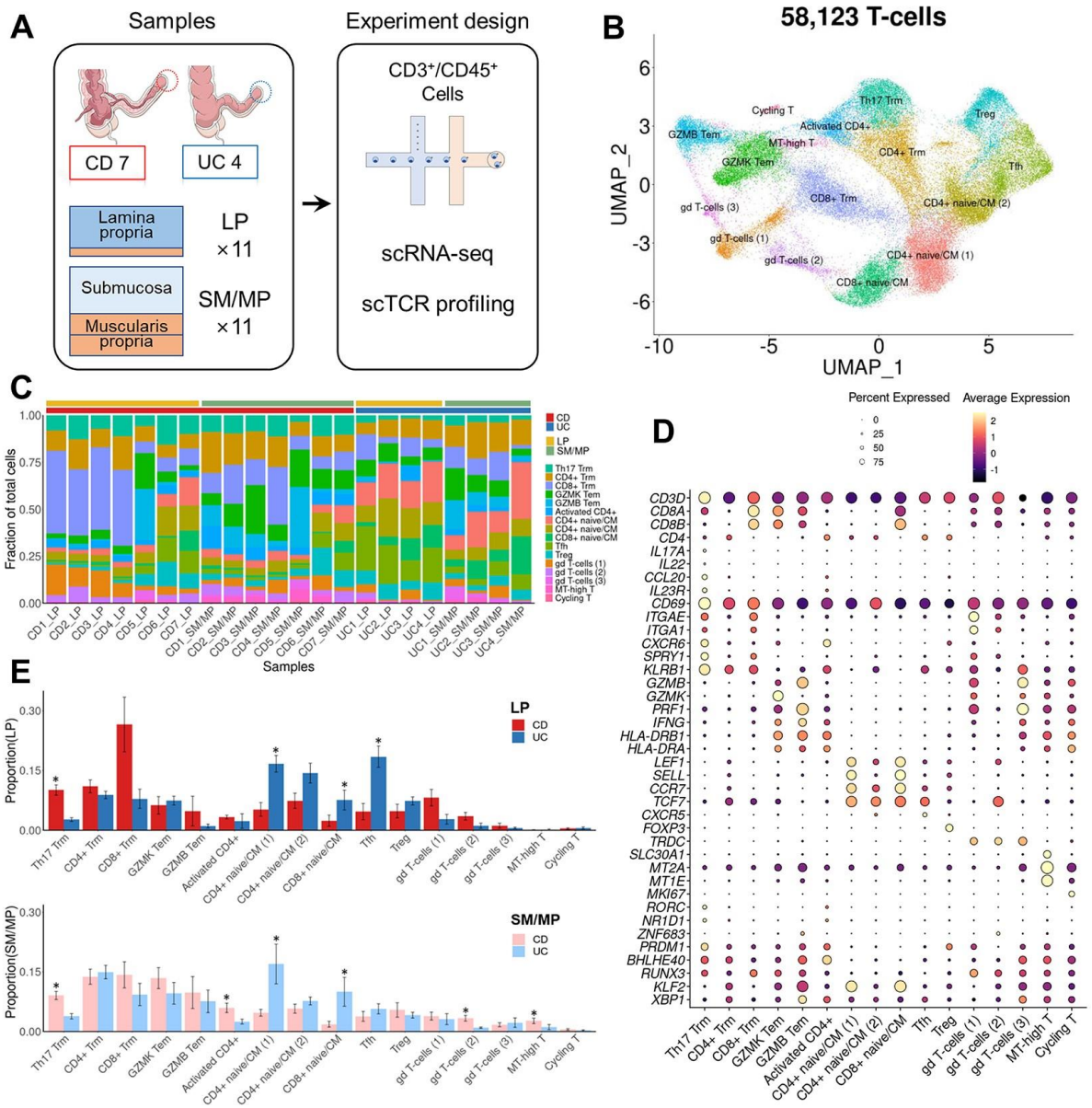

Figure 2. Single-cell transcriptome profiling of T cells. (A) A study design. (B) UMAP (Uniform manifold approximation and projection) plot of all sorted T cells. (C) Frequency of 16 major T cell subpopulations in each sample included in the scRNA-seq analysis. The bar at the top of the heatmap represents the disease states and location information of each sample. (D) Dot plot showing expression level and percentage of expressed cells for selected marker genes for T cell subsets. (E) Bar plots showing differences in cell type proportion for CD and UC samples in LP (up) and SM/MP (down) (*P < 0.05 for Wilcoxon rank sum test). CM, central memory; em, effector memory; fh, follicular helper; gt, gamma delta; MT, metallothionein; reg, regulatory; rm, resident memory.

3.2 Transcriptional regulatory mechanisms

Expanding upon these findings, our study delved into the intricate transcriptional network analysis governing distinct T cell states. By computing coexpression modules for each gene and identifying potential target genes for each TF, we successfully identified 327 TF regulatory modules (regulons) spanning all 16 T cell clusters. Activity scores for each identified regulon were computed across the entire spectrum of T cells, revealing cluster-specific activities across several regulons and providing further insights into distinct transcriptional regulation patterns among different Trm clusters (Figure 3A-B).

Within the Th17 Trm cluster, specific regulon activities associated with *RORC* and *NR1D1* were observed (Figure 4A), transcription factors closely linked to Th17 cell differentiation.[25,26] These findings are in alignment with previous research,[25] indicating that the transcriptional repressor *NR1D1* competes with RORγt for their shared DNA consensus sequence and negatively regulates Th17 cell development. Higher expression levels of *RORC* were observed in long-lived Th17 Trm and exhausted Th17 Trm cells compared to other $CD4^+$ T cells in mice,[27] further corroborating the distinctive characteristics of the Th17 Trm cluster in perpetuating the Th17 response and maintaining Th17 cell functions.

3.3 Heightened Th17 Trm population in CD

Given the substantial increase in the Th17 Trm population in CD, we performed a comprehensive analysis of their distinct transcriptional characteristics. Recognizing the comparable transcriptional features shared among the three Trm clusters in LP and SM/MP (Figure 5), we integrated these Trm clusters across both locations. Subsequently, we conducted a DE analysis involving three Trm clusters: Th17 Trm vs. $CD4^+$ Trm, Th17 Trm vs. $CD8^+$ Trm, and $CD4^+$ Trm vs. $CD8^+$ Trm (Figure 4B). This analysis identified a unique set of 300 genes referred to as DEGs, present in at least one of the three comparative analyses, highlighting significant transcriptional variations within the expanded Th17 Trm clusters. The analysis revealed markedly elevated expression levels of hallmark Th17 markers, such as *IL17A* and *IL22*, as well as cytotoxic molecules like *GZMA* and *NKG7* in the amplified Th17 Trm compared to the $CD4^+$ Trm, emphasizing the pronounced inflammatory signatures within Th17 Trm. Conversely, $CD4^+$ Trm exhibited heightened expression of quiescent markers such as *TCF7*, *SELL*, and *KLF2*. In the comparison between Th17 Trm and $CD8^+$ Trm, upregulation of Th17-associated genes was observed in Th17 Trm, similar to the comparison with $CD4^+$ Trm, and higher expression of $CD8^+$ effector-related transcripts such as *CXCR3* and *KLRD1* was found in the $CD8^+$ Trm. The analysis revealed distinct gene expression patterns associated with cytokines and their receptors, highlighting the differences between the amplified Th17 Trm clusters (Figure 4C). This suggests significant variations in chemokine receptor expression among the Trm populations, influencing their potential

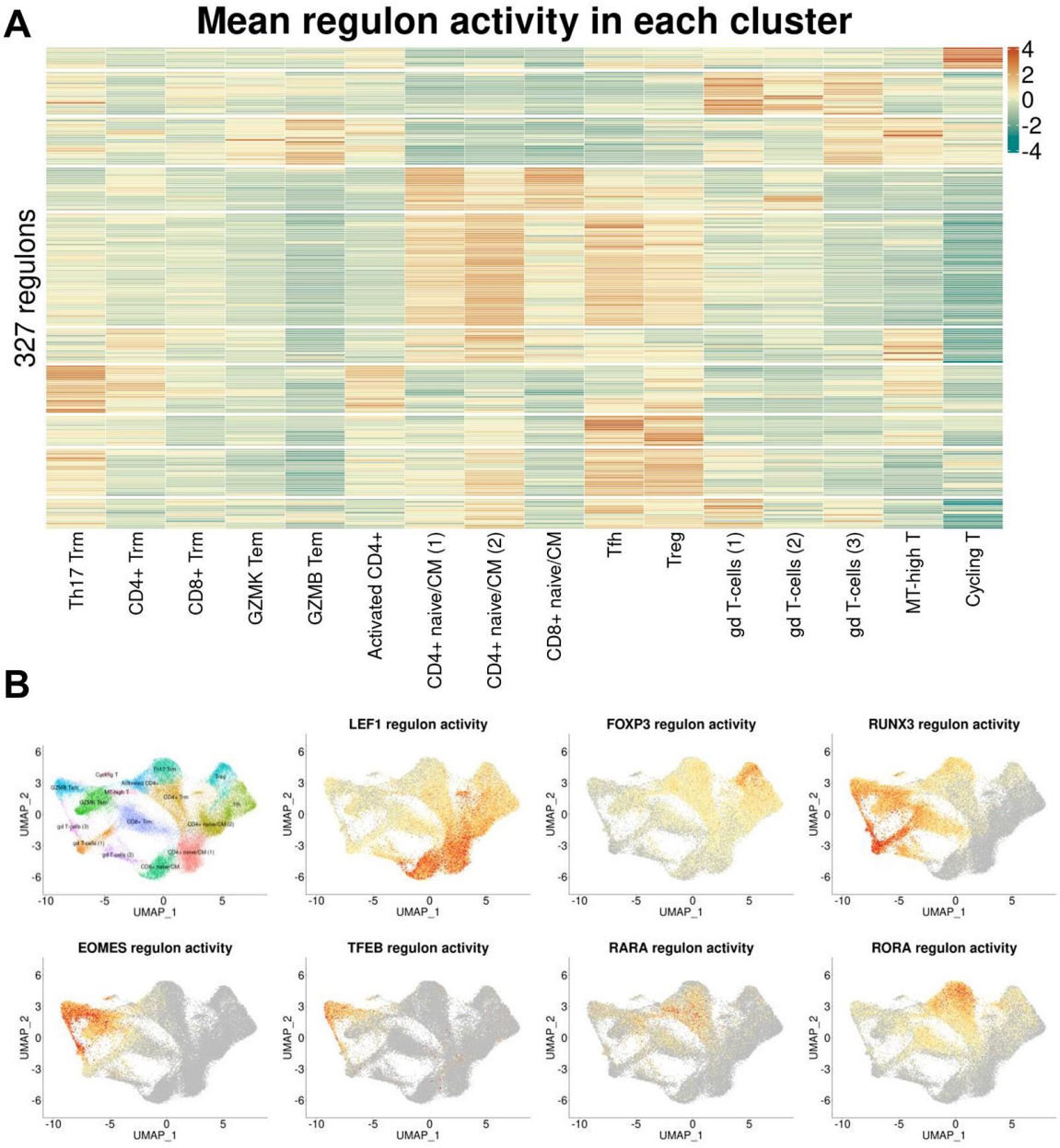

Figure 3. Relative regulon activity for detected transcription factor modules. (A) Heatmap visualizing relative regulon activity for all detected transcription factor modules in 16 clusters. (B) Distribution of selected transcription factor regulon activity scores of each cell on UMAP.

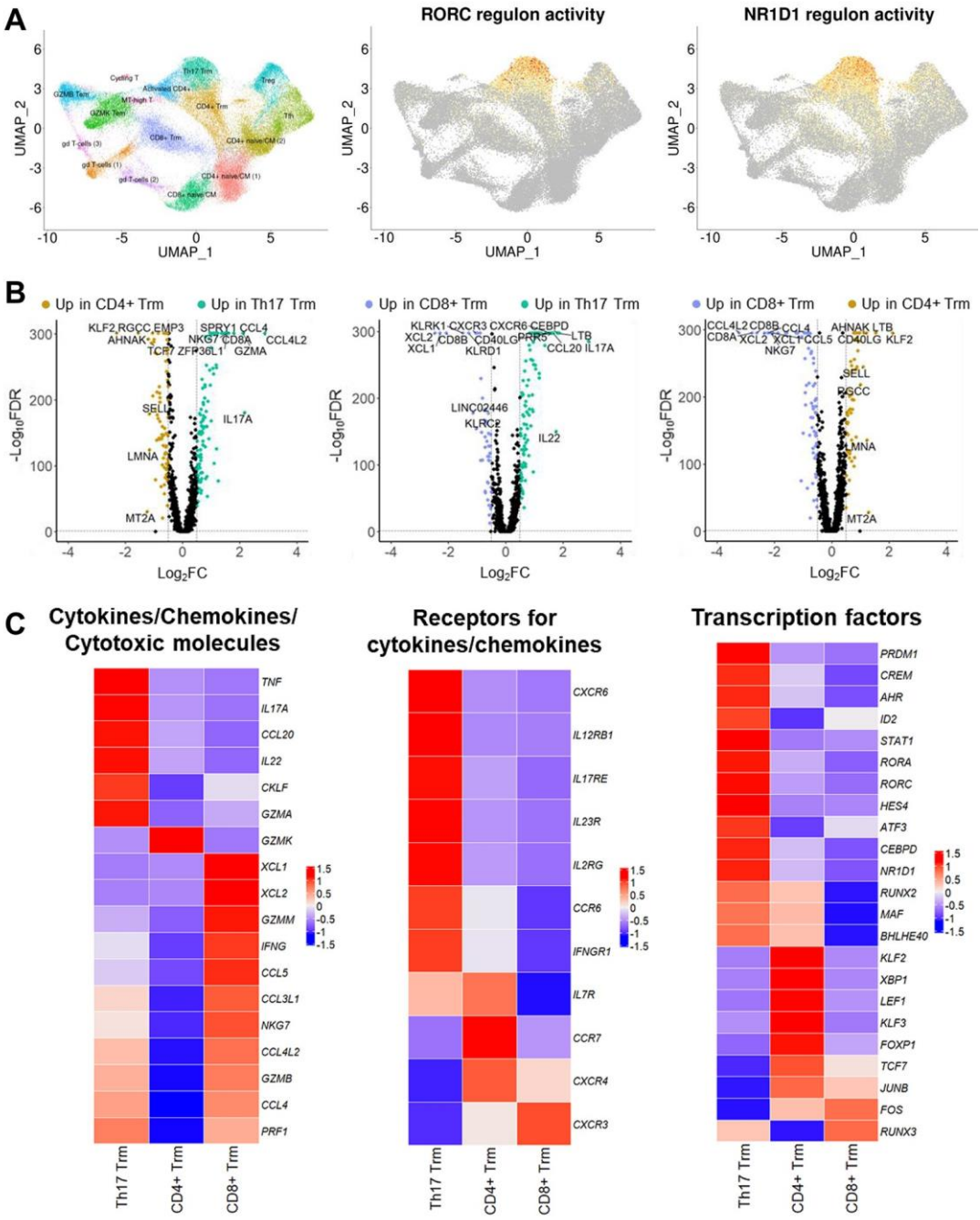

Figure 4. Transcriptional differences between tissue-resident memory T cells. (A) Distribution of *RORC* and *NR1D1*, transcription factors closely linked to Th17 cell differentiation, regulon activity scores of each cell on UMAP. (B) Volcano plots showing the results of differential expression (DE) analysis for $CD4^+$ Trm vs. Th17 Trm (left), $CD8^+$ Trm vs. Th17 Trm (mid) and $CD8^+$ Trm vs. $CD4^+$ Trm (right). In each volcano plot, the colored genes represent statistically significant differentially expressed genes (DEGs). (C) Expression levels of cytokines/chemokines/cytotoxic molecules, receptors for cytokines/chemokines, and transcription factors in each Trm cluster. Each category included only genes identified as significant DEGs at least once among the results of DE analysis.

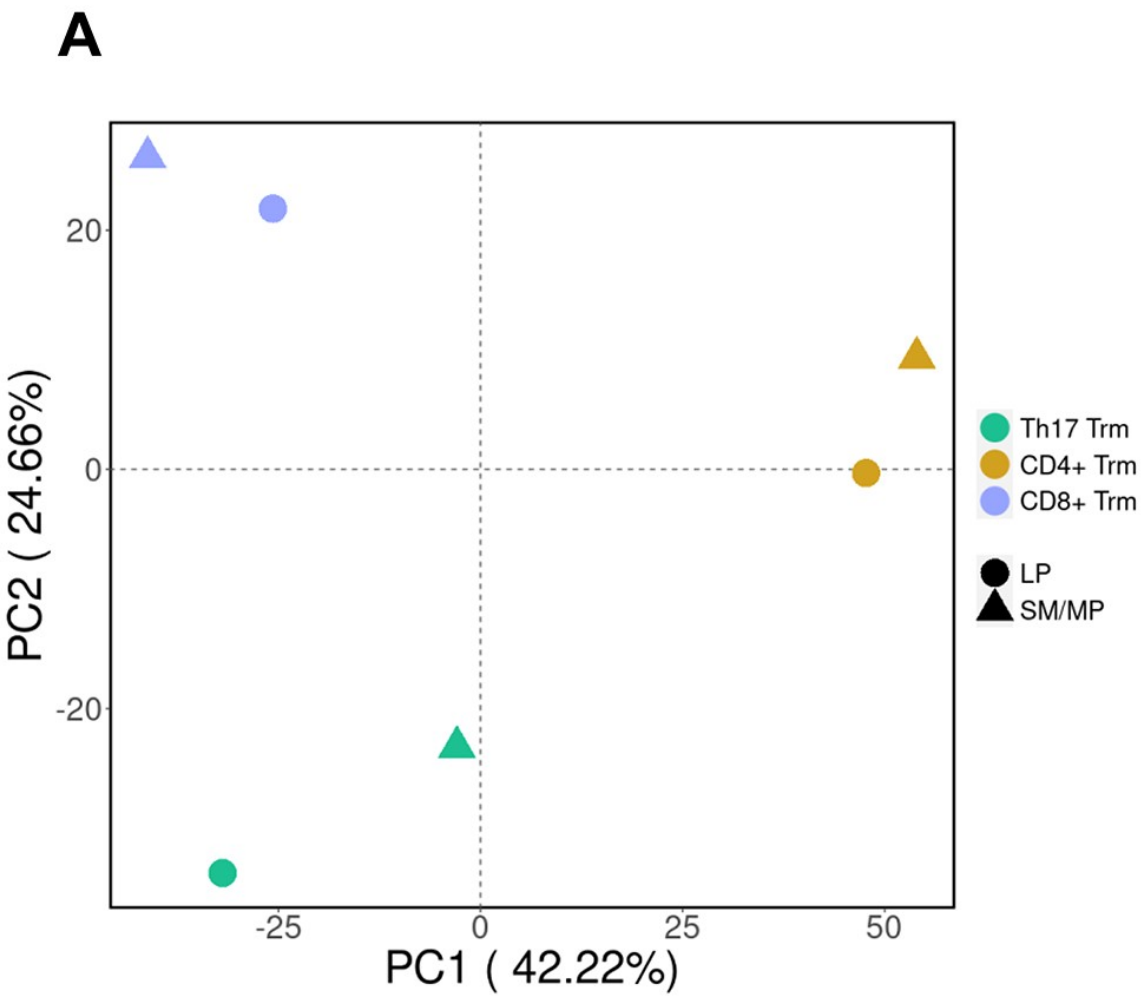

Figure 5. Principal component analysis of pseudobulk gene expression for three Trm clusters. Principal component analysis of pseudobulk gene expression using top 1,000 highly variable genes for three Trm clusters.

for specific location trafficking. Notable examples include genes related to Th17-specific migration, such as *CXCR6* and *CCR6*, which were prominently expressed in the amplified Th17 Trm cluster.[28] Moreover, both *CCR6* and its ligand *CCL20* exhibited increased expression, indicating upregulation of this receptor-ligand pair in Th17 Trm cells. Based on the supportive evidence from the preceding analysis (Figure 4A), variations in TF expression were evident across different amplified Th17 Trm clusters, with several TFs displaying elevated expression consistent with established Th17-specific signatures (Figure 4C).[29]

3.4 Mapping T cell trajectories and clonal dynamics

To understand the intricate transitions among T cell clusters, we conducted pseudotime trajectory analyses in both $CD4^+$ and $CD8^+$ compartments using diffusion maps. In the $CD4^+$ compartment, the $CD4^+$ naive/CM (1) and $CD4^+$ naive/CM (2) clusters marked the initial stages of the trajectory. This unveiled two distinct branches: one leading to the Th17 Trm cluster, flanked by the activated $CD4^+$ cluster and the $CD4^+$ Trm cluster, and the other including the regulatory T (Treg) and follicular helper T (Tfh) clusters (Figure 6A). These findings highlight the unique trajectory of Th17 Trm transitioning from Treg or Tfh states in the $CD4^+$ lineage.

Using TCR data from each cell, we also assessed clonality to explore shared clonotypes across various T cell clusters and to establish a connection between clonal expansion and T cell activation. Notably, the Th17 Trm cluster exhibited extensive clonotype sharing with other clusters in the $CD4^+$ T cell compartment, sharing 127 and 59 clonotypes with the $CD4^+$ Trm cluster and the activated $CD4^+$ cluster, respectively, and 31 clonotypes across all three clusters (Figure 6B). To quantify state transitions between T cell clusters, we calculated transition scores using clonotypes shared by different clusters ($P = 1.13 \times 10^{-4}$, Kruskal–Wallis test). A comparison of transition scores in $CD4^+$ T cell clusters between CD and UC revealed a more active state transition of Th17 Trm in patients with CD (Th17 Trm-$CD4^+$ Trm, $P = 6.06 \times 10^{-3}$; Th17 Trm- activated $CD4^+$, $P = 4.24 \times 10^{-2}$; two-sided Wilcoxon rank-sum test, Figure 6C). The Th17 Trm cluster stood out from the $CD4^+$ T cell clusters, with nearly 25% of cells categorized as highly expanded (Figure 6D). This contrasted with the mostly unexpanded state observed within $CD4^+$ naive/CM clusters, the Tfh cluster, and the Treg cluster. In the LP samples, a significant difference in expansion scores emerged between the CD and UC samples ($P = 0.006$, Wilcoxon rank-sum test) within the Th17 Trm cluster (Figure 6E). These findings suggest a substantial enhancement in the clonal expansion of Th17 Trm cells within the small bowel of CD, particularly in the LP region.

In the $CD8^+$ compartment, we observed a transition from $CD8^+$ Trm to GZMB effector memory (Tem) cells, with GZMK Tem acting as an intermediary (Figure 7A). A substantial clonotype overlap occurred between the GZMK Tem and GZMB Tem clusters, with 116

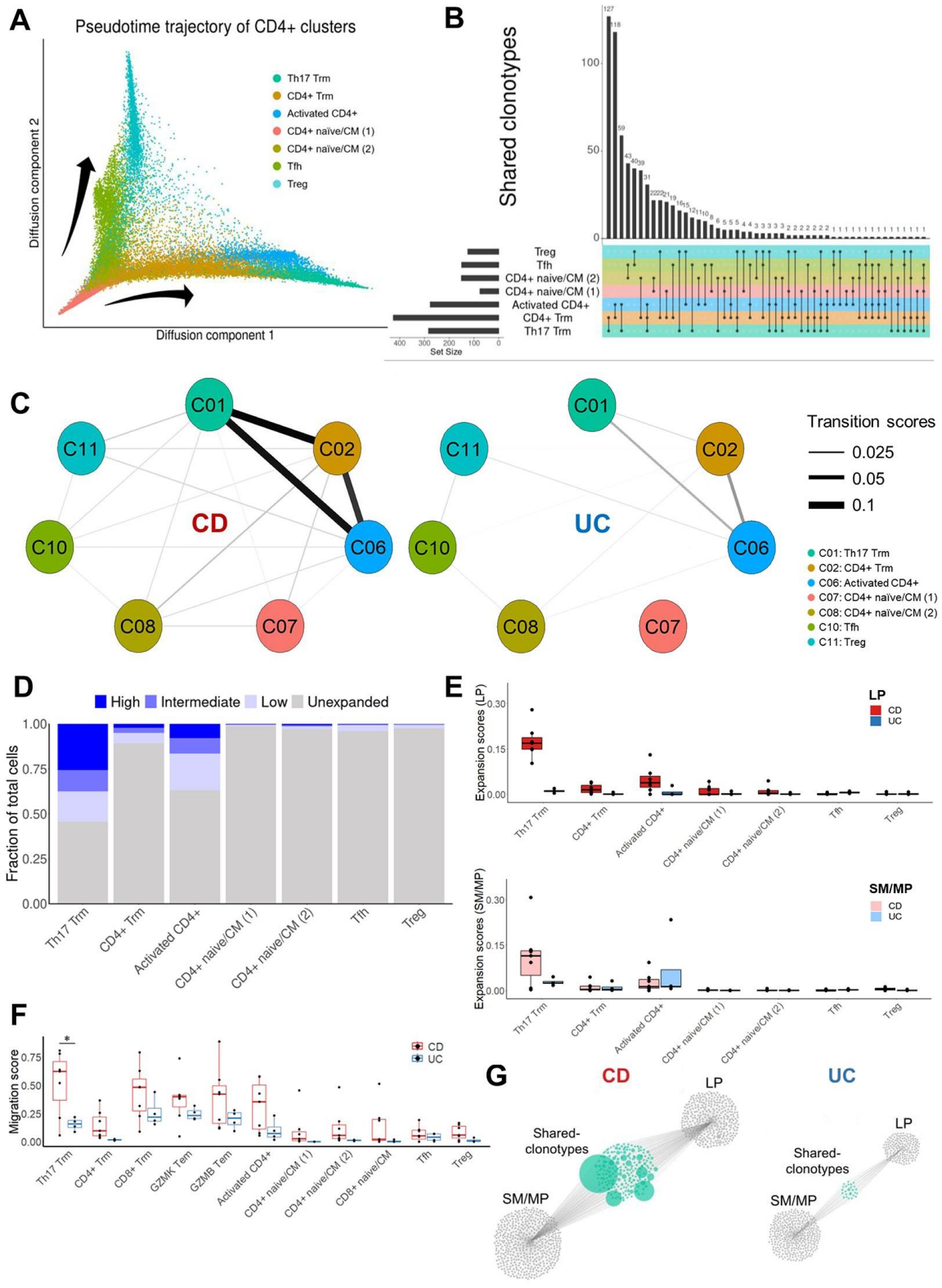

Figure 6. CD4$^+$ T cell trajectories and clonal dynamics. (A) The pseudotime trajectory of CD4$^+$ clusters in a diffusion map using two diffusion components. Each colored dot indicated cells of different clusters. (B) UpSet plot representing the number of shared clonotypes between cells of different CD4$^+$ clusters. Black circles connected by a black line means that shared clonotypes exist

in the connected clusters. The number above the top bar indicates the number of shared clonotypes between the clusters. The bar on the left of each cluster represents the number of unique clonotypes in each cluster. (C) Cross-cluster phenotypic transition scores of $CD4^+$ clusters in each disease state. The thickness of the line represents a measure of clonotype sharing between two different clusters. (D) A bar plot showing the TCR clonality of each $CD4^+$ cluster. Only cells with CDR3 information, following quality control for TCR profiling, are included. (E) Expansion scores for all $CD4^+$ clusters quantified by STARTRAC for each sample. (F) Migration scores for all clusters quantified by STARTRAC for each patient. Clusters with fewer than 100 cells per location were excluded from the analysis. (G) Clonal networks of TCR repertoires in the Th17 Trm are depicted. Each dot represents a clonotype defined by the CDR3 sequence of TCR-beta. Connecting lines indicate shared clonotypes between LP and SM/MP. The dot size indicates the clonal expansion of each clonotype.

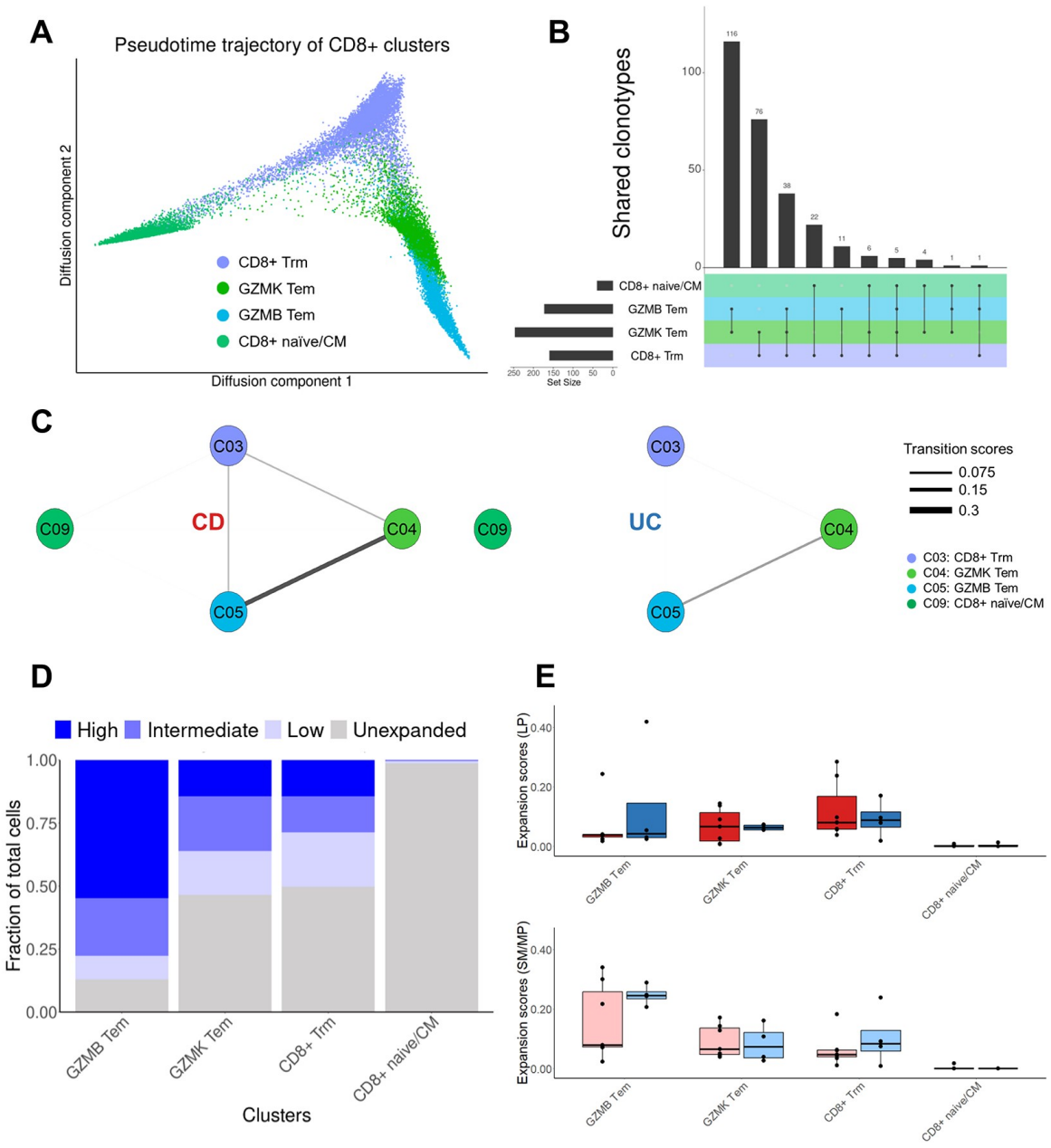

Figure 7. CD8$^+$ T cell trajectories and clonal dynamics. (A) The pseudotime trajectory of CD8$^+$ clusters in a diffusion map using two diffusion components. Each colored dot indicated cells of different clusters. (B) UpSet plot representing the number of shared clonotypes between cells of different CD8$^+$ clusters. Black circles connected by a black line means that shared clonotypes exist in the connected clusters. The number above the top bar indicates the number of shared clonotypes between the clusters. The bar on the left of each cluster represents the number of unique clonotypes in each cluster. (C) Cross-cluster phenotypic transition scores of CD8$^+$ clusters in each disease states. The thickness of the line represents a measure of clonotype sharing between two different clusters. (D) A bar plot showing the TCR clonality of each CD8$^+$ cluster. (E) Expansion scores for all CD8$^+$ clusters quantified by STARTRAC for each sample.

shared clonotypes. Interestingly, the number of shared clonotypes between $CD8^+$ Trm and GZMK Tem was approximately seven times higher than that between $CD8^+$ Trm and GZMB Tem (Figure 7B-C). When combined with insights from the pseudotime trajectory analysis of the $CD8^+$ T cell clusters, these findings suggest that GZMK Tem may represent transitional states bridging the gap between $CD8^+$ Trm and fully differentiated GZMB Tem cells. The GZMB Tem cluster exhibited significant clonal expansion, aligning with its position as the terminal cluster in the pseudotime trajectory analysis (Figure 7D).

3.5 T cell clonotype dynamics across gut compartments

Considering the established migratory capacity of T cells throughout the bowel layers in response to antigens,[9] we investigated the migratory tendencies of T cells within each patient by quantifying shared clonotypes in paired samples. Migration scores were computed for each patient, revealing a notable disparity in migration scores between CD and UC samples solely within the Th17 Trm cluster (Figure 6F). In patients with CD, most of the expanded clonotypes in Th17 Trm were shared between the LP and SM/MP samples (Figure 6G). These findings suggested that the extensive sharing of Th17 Trm clonotypes in paired samples from CD patients was linked to their increased clonal expansion, highlighting their strong capability for dynamic interstitial migration within the small bowel microenvironment. Notably, the $CD8^+$ clusters exhibited no notable discrepancies in expansion scores across all clusters when comparing CD and UC samples, spanning both LP and SM/MP regions (Figure 7E).

3.6 Exploring shared CDR3 sequences

Given the crucial role of TCR-beta CDR3 clonotypes in recognizing specific antigens within the T cell repertoire, our aim was to identify shared CDR3 sequences among patients with CD, potentially indicating priming for the inflammatory response. While a notable portion of CDR3 sequences was shared within paired samples from the same patient, the number of sequences exhibiting sharing across distinct CD patients was limited to five or fewer (Figure 8A). Considering the scarcity of shared CDR3 sequences among patients, we further employed GLIPH (Grouping of Lymphocyte Interactions by Paratope Hotspots) to identify TCR motifs based on CDR3 similarity.[30] We identified 40 TCR motifs, each comprising at least 10 different CDR3 sequences. The largest TCR motif encompassed a total of 1,258 CDR3 sequences from 1,856 cells. However, it is noteworthy that specific TCR motifs exclusive to clusters or patients with CD remained elusive within our observations (Figure 8B).

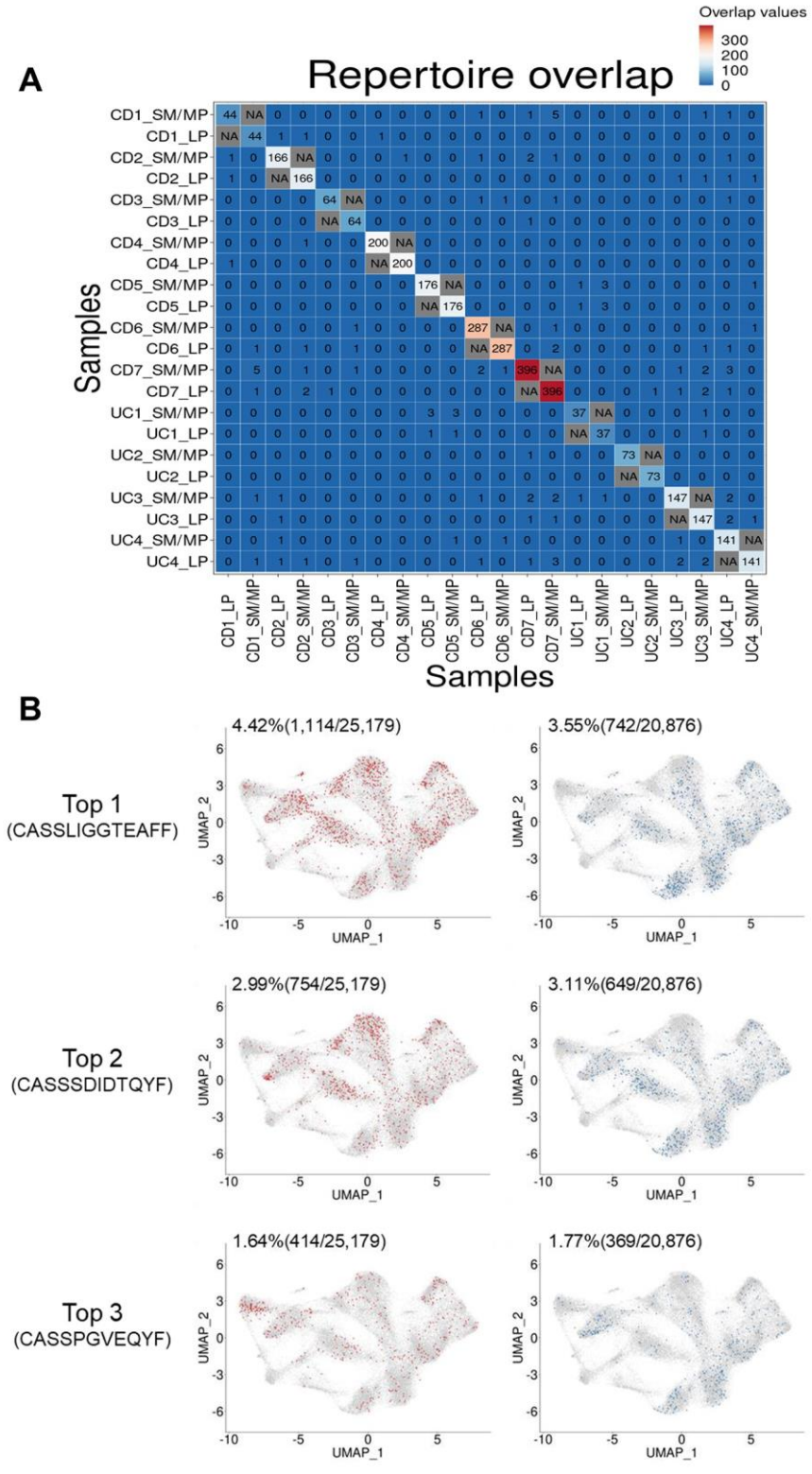

Figure 8. Shared CDR3 sequences among patients with CD or UC. (A) Heatmap showing the overlapping TCR repertoire of each sample. The numbers in heatmap indicate the number of clonotypes shared between different samples. (B) The top three TCR motifs containing the most CDR3 sequences among the total 40 TCR motifs identified by GLIPH. Cells from CD patients (left) and UC patients (right) with each TCR motifs are shown on UMAP.

3.7 CD-prominent Th17 Trm engages in crosstalk with immune cells

To examine the transcriptional changes of Trm clusters in CD, we identified DEGs in the CD vs. UC analysis, followed by gene set enrichment analysis based on the gene list derived from the DEGs. CD patients exhibited significant upregulation of immune-related pathways in three Trm clusters (Figure 9A). Importantly, the Th17 Trm cluster, specifically in CD patients, showed a distinctive surge in the interferon gamma (IFNγ) production pathway, exhibiting notable expression disparities in genes associated with IFNγ production and response within this cluster (Figure 9B).

To examine the impact of heightened IFNγ expression by Th17 Trm on neighboring immune cell populations in CD, we conducted clustering analysis targeting $CD45^+$ immune cells (Figure 9C-D and Figure 10A-C). Our assessment of the IFNγ response highlighted significant differences in myeloid and T cell clusters within the LP, suggesting a stronger influence of elevated *IFNG* expression on immune cells in this region compared to the SM/MP areas (Figure 9C). Given the intricate ligand-receptor interactions among diverse immune cells, our application of the NicheNet R package helped elucidate the crosstalk between Th17 Trm and myeloid cells.[21] We used a target gene by identifying a gene list with heightened expression in myeloid cells of CD patients compared to UC patients and predicted Th17 Trm ligands driving these changes. Among the ligands expressed in the Th17 Trm, it was confirmed that *IFNG* was the best predictor of genes with increased expression in myeloid cells of patients with CD (Figure 9D). In addition, various inflammatory cytokines such as *TNF* and *IL1B* showed high prediction scores for changes in gene expression of myeloid cells. Chemokines such as *CXCL10*, *CXCL8*, and *CXCL9* expressed in myeloid cells were predicted to be strongly induced by *IFNG* (Figure 9D). Overall, it is thought that IFNG, whose expression is increased in Th17 Trm of patients with CD, increases inflammatory signatures in myeloid cells and consequently may contribute to inflammation.

3.8 Role of *STAT1* in proinflammatory Th17 Trm

Our hypothesis of the heightened Th1-like characteristics of CD-prominent Th17 Trm, in comparison to UC, was validated by the increased expression of the key Th1 transcription factor *STAT1* in CD. Further supporting this observation, the analysis of TF module scores related to IFNγ signaling revealed significantly higher scores for the induced *STAT1*/*IRF1* axis TF modules in patients with CD (Figure 9E).[31,32] Genes with heightened expression in CD patients were notably linked to immune pathways, particularly the IFNγ response (Figure 9F), in line with prior research suggesting the acquisition of Th1-like attributes by pathogenic Th17 cells.[5,32] Categorizing Th17 Trm into groups based on *STAT1* and *IRF1* expression, we observed significant differences in CD vs. UC proportions within each group (Figure 9G). Notably, CD patients exhibited a higher proportion of $STAT1^+$ Th17 Trm cells regardless of *IRF1* expression, while the $STAT1^-$ group was more prevalent in UC patients.

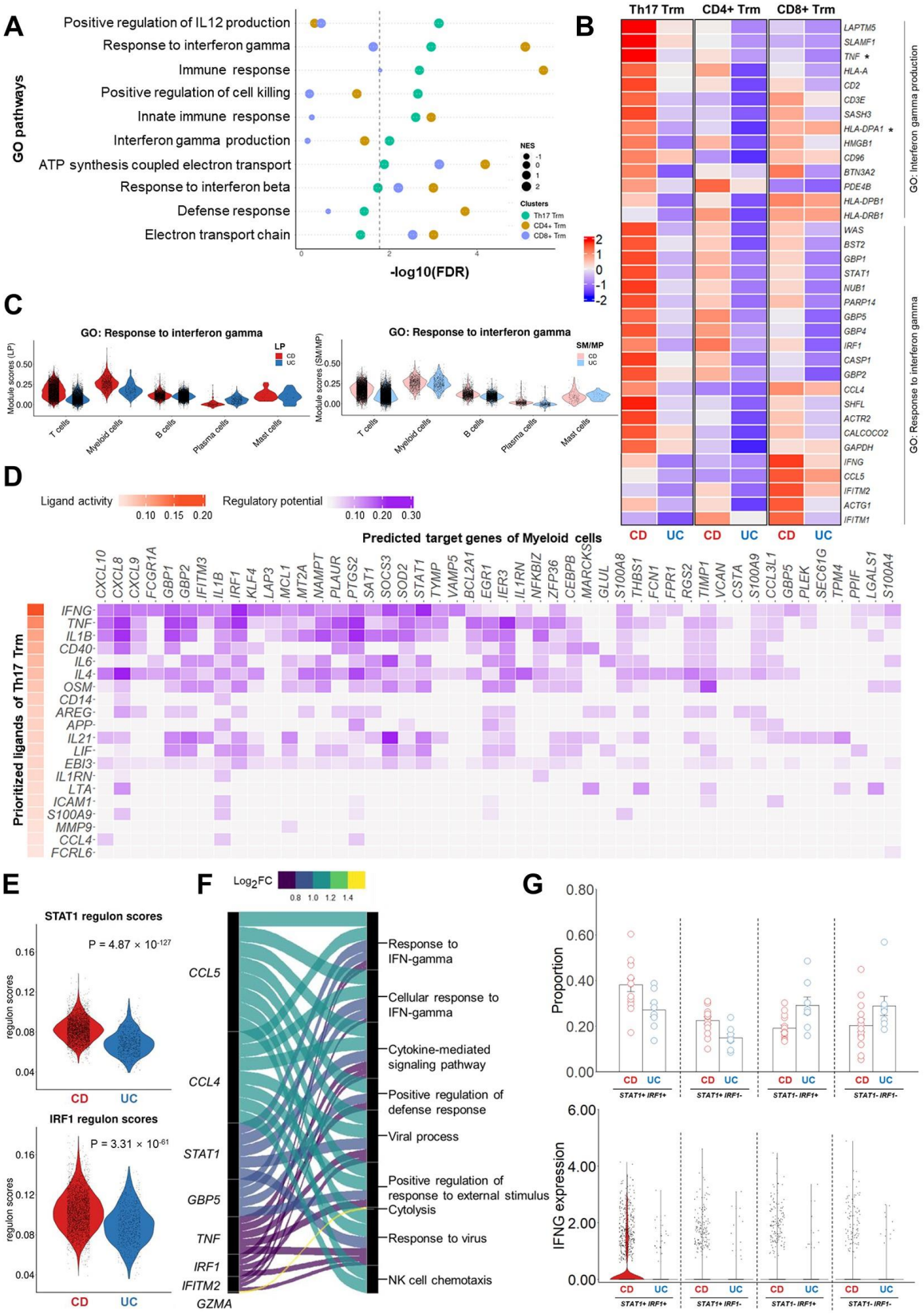

Figure 9. Impact of heightened IFNγ expression by Th17 Trm on neighboring immune cells. (A) Dot plot of enrichment analysis of differentially expressed genes (DEGs) between CD and UC in Th17 Trm cluster (green), CD4$^+$ Trm cluster (brown), and CD8$^+$ Trm cluster (blue). Sizes of the circle

indicate the normalized enrichment score (NES) for each pathway in the three Trm clusters. (B) A heatmap showing the expression level of genes belonging to the interferon gamma (IFNγ) production or response to IFNγ pathways by disease state in the three Trm clusters. Asterisks indicate genes belonging to both pathways. (C) Violin plots showing modules scores for response to IFNγ pathway in different $CD45^+$ clusters. (D) Ligand activity prediction in Th17 Trm cluster for genes with elevated expression in myeloid cells of patients with CD using the NicheNet R package. The NicheNet pipeline matches secreted ligands with their corresponding receptors and scores their regulatory potential on a defined gene set. The results show the top 20 ligands predicting the differentially expressed genes (DEGs) in myeloid cells. The ligand-target matrix illustrates the intricate crosstalk between Th17 Trm and myeloid cells. (E) Violin plots showing regulon scores by disease state in Th17 Trm cells. (F) Alluvial plot connecting the top enriched Gene Ontology (GO) biological processes with regulon genes (Figure 9E) which significantly upregulated in CD vs. UC in Th17 Trm; Flows colored according to fold change. (G) A bar plot (up) showing the proportion of each group according to the expression level of *STAT1* and *IRF1* and a violin plot (down) showing the expression level of *IFNG*.

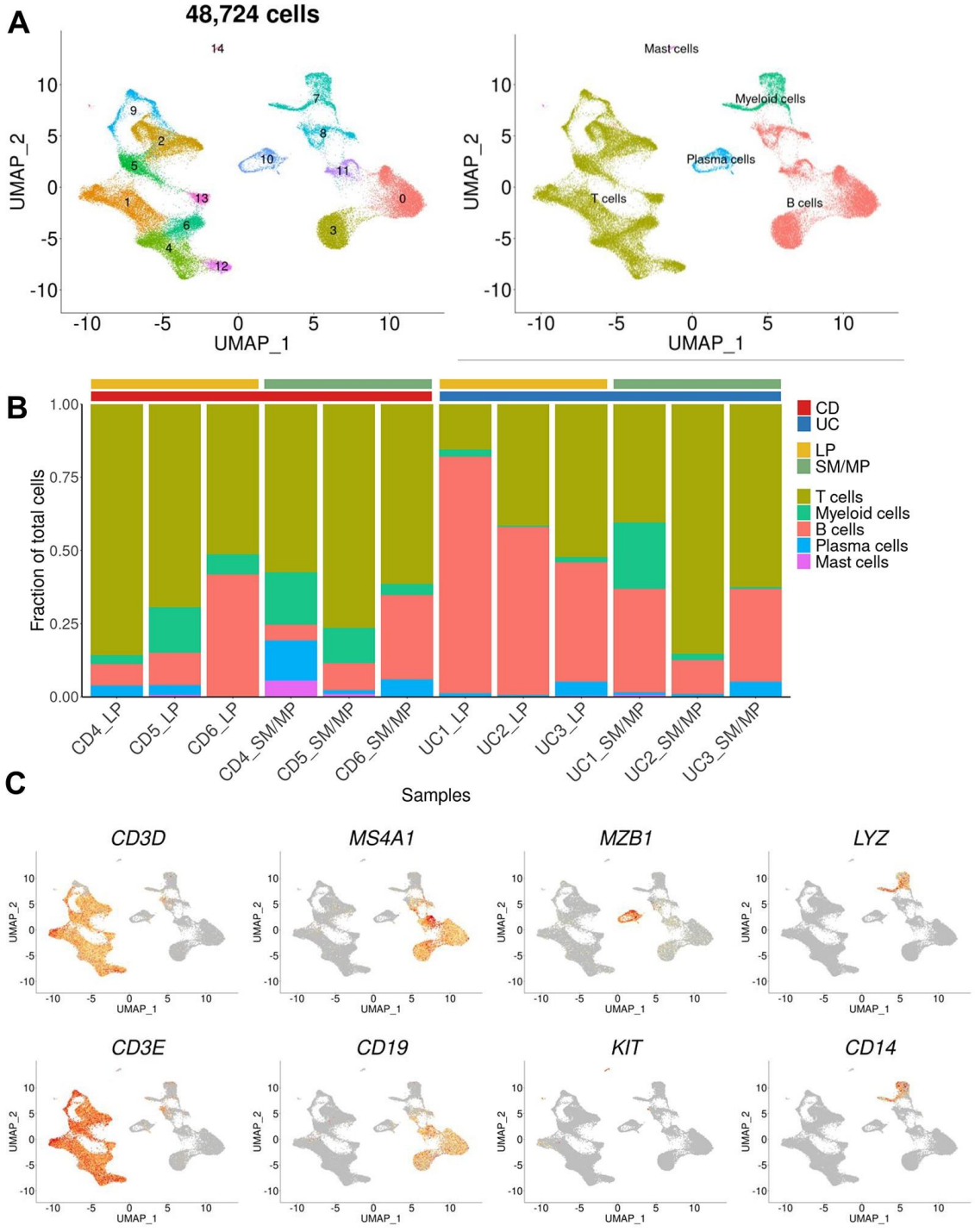

Figure 10. Single-cell transcriptome profiling of CD45$^+$ immune cells. (A) UMAP plot of CD45$^+$ cells from six samples (three CD and three UC patients). We categorized diverse immune cell types, including T cells, B cells, plasma cells, myeloid cells, and mast cells, revealing a total of 48,724 cells. (B) Frequency of five major CD45$^+$ populations in each sample included in the CD45$^+$ scRNA-seq analysis. The bar at the top of the heatmap represents the disease states and location information of each sample. (C) Marker expression of CD45$^+$ immune cells.

Importantly, the *STAT1*$^{+}$ *IRF1*$^{+}$ subgroup showed significant differences in *IFNG* expression exclusively between CD and UC patients (Figure 9G). These findings underscore the possible roles of *STAT1* and *IRF1* in driving the heightened Th1 signatures within the Th17 Trm population of CD patients.

4. DISCUSSION

Our study utilized scRNA-seq and paired scTCR-seq to investigate Trm cells in the small bowel of patients with CD. Reflecting the transmural nature of CD, our findings highlighted the retention and significant clonal expansions of Th17 Trm cells in both the LP and SM/MP regions. Transcriptome analysis revealed pro-inflammatory markers in these cells, including increased IFNγ, which enhanced inflammatory signatures in myeloid cells, suggesting their potential involvement in chronic inflammation.

Trm cells have been considered as potential contributors to the chronic relapsing and remitting nature of autoimmune diseases.[2] In psoriasis, Trm cells have been known to persist and contribute to the recurrence of skin lesions, even after successful treatment.[33,34] Similarly, in CD, recurrences often occur at the site of anastomosis following bowel resection, suggesting a potential role for Trm cells in the pathology of CD. Therefore, it is essential to understand Trm cells under steady-state conditions in the context of CD. We observed a quantitative enrichment of Th17 Trm cells in the small bowel of patients with CD. These Th17 Trm cells exhibited an increased production of IFNγ, with a pronounced presence in the LP compared to the SM/MP regions. This observation aligns with the increased presence of ex-Th17 cells found in the synovial fluid of patients with RA.[35] Significant elevation of *IFNG* expression was observed in the *STAT1*$^{+}$ subgroup of the Th17 Trm in CD (Figure 9G), indicating the potential role of *STAT1* in regulating these augmented Th1 signatures within the Th17 Trm population. Additionally, we predicted that IFNγ induced the production of chemokines like *CXCL10*, *CXCL8*, and *CXCL9* in myeloid cells. These collective findings suggested that *IFNG*, upregulated in Th17 Trm of CD and associated with *STAT1* activation, significantly contributed to enhanced inflammatory signatures within myeloid cells, providing a compelling rationale for the utility of targeting the JAK-STAT pathway for the maintenance treatment of CD.

CD4^{+} T cells have been implicated in various autoimmune conditions, including CD, psoriasis, multiple sclerosis, and rheumatoid arthritis, often displaying a Th17 or Th1-Th17 hybrid phenotype.[2,36] However, the role of elevated IL-17 in CD pathogenesis is still unclear. Therapeutics targeting the IL-23-IL-17 pathway have shown effectiveness in CD treatment, while IL-17A blockade has been less successful in CD and rheumatoid arthritis.[37,38] These results may be attributed to the pleiotropic effects of IL-17A,[2,39,40] which not only induces inflammation[41,42] but also promotes intestinal epithelial barrier function[43] and repair, and participates in an autoregulatory loop to limit the pathogenicity of Th17 cells.[44] The plasticity of Th17 cells, influenced by various factors including T cell-polarizing cytokines and the inflammatory tissue environment, is crucial in maintaining gut mucosal homeostasis. In CD, the limited effectiveness of drugs targeting IL-17A may be linked to the presence of ex-Th17 cells that switch to producing IFNγ.[40,45] These cells could play a role in the

pathology of CD, suggesting that targeting these alterations might offer a more effective approach to reducing inflammation.

Our study has several limitations. Firstly, since our CD patient samples were limited to non-inflamed regions, preventing us from assessing the role of Th17 Trm cells in inflamed tissues. We also identified shared clonotypes between Th17 Trm and adjacent $CD4^+$ T cell clusters, yet this did not fully elucidate Th17 Trm differentiation during CD pathogenesis. Although we attempted sub-clustering analysis of Th17 Trm to confirm their origin from activated Th17 cells, the limited number of Th17 Trm cells hindered clear sub-cluster delineation based on activation state. Nevertheless, the presence of elevated scores for Th17-related regulon modules in the Th17 Trm cluster suggested that Th17 Trm might originate from activated Th17 cells. Secondly, the absence of microbiome data prevented us from linking specific microbiomes known to be associated with Th17 cell development to the increased presence of Th17 Trm cells in CD patients.[46] Additionally, we could not confirm the interaction between Th17 Trm cells and cells forming the intestinal barrier, such as epithelial cells. Furthermore, our non-CD controls consisted of patients with UC, which could introduce a potential selection bias. However, considering the remarkably similar transcription profiles observed in previous bulk RNA analyses,[47] we believe that they can be considered suitable controls for the purposes of this study. Lastly, due to the lack of histological data, assessing the influence of microscopic inflammation within the tissues on our study findings was challenging. Nevertheless, we attempted to overcome this limitation by calculating molecular scores based on inflammation-associated gene signatures,[48] which did not reveal significant differences among the samples (Figure 11).

In summary, our study illuminates the clonal expansion and activation of Th17 Trm cells in the small bowel of patients with CD, indicating their potential role in CD pathogenesis. Furthermore, we revealed distinctive expression patterns of chemokine receptors and their ligands in Th17 Trm cells and immune cells, emphasizing their pivotal role in cellular communication and migration within the inflammatory microenvironment. These findings deepen our comprehension of the immune landscape in CD and hold promise for the development of targeted therapeutic strategies aimed at modulating Th17 Trm cell responses and their interactions with immune cells.

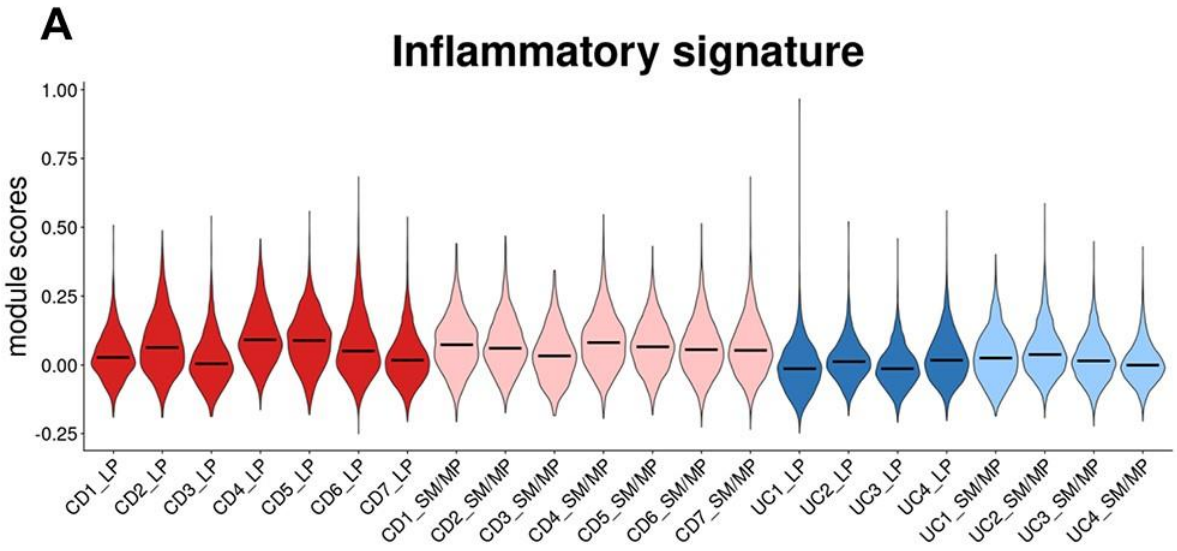

Figure 11. Inflammatory signature scores for each sample. Inflammatory signature scores calculated using the following inflammatory-associated genes for each sample (Smillie CS et al. Cell 2019): *IFNG*, *IFNGR1*, *IFNGR2*, *IL10*, *IL12A*, *IL12B*, *IL12RB1*, *IL12RB2*, *IL13*, *IL17A*, *IL17F*, *IL18*, *IL18R1*, *IL18RAP*, *IL1A*, *IL1B*, *IL2*, *IL21*, *IL21R*, *IL22*, *IL23A*, *IL23R*, *IL2RG*, *IL4*, *IL4R*, *IL5*, *IL6*, *JUN*, *NFKB1*, *RELA*, *RORA*, *RORC*, *S100A8*, *S100A9*, *STAT1*, *STAT3*, *STAT4*, *STAT6*, TGFB1, *TGFB2*, *TGFB3*, and *TNF*.

References

1. Gordon H, Rodger B, Lindsay JO, et al. Recruitment and Residence of Intestinal T Cells - Lessons for Therapy in Inflammatory Bowel Disease. J Crohns Colitis 2023;17:1326-1341.
2. Oja AE, van Lier RAW, Hombrink P. Two sides of the same coin: Protective versus pathogenic CD4(+) resident memory T cells. Sci Immunol 2022;7:eabf9393.
3. Zundler S, Becker E, Spocinska M, et al. Hobit- and Blimp-1-driven CD4(+) tissue-resident memory T cells control chronic intestinal inflammation. Nat Immunol 2019;20:288-300.
4. DeWolf S, Elhanati Y, Nichols K, et al. Tissue-specific features of the T cell repertoire after allogeneic hematopoietic cell transplantation in human and mouse. Sci Transl Med 2023;15:eabq0476.
5. Schnell A, Huang L, Singer M, et al. Stem-like intestinal Th17 cells give rise to pathogenic effector T cells during autoimmunity. Cell 2021;184:6281-6298.e6223.
6. Shin B, Kress RL, Kramer PA, et al. Effector CD4 T cells with progenitor potential mediate chronic intestinal inflammation. J Exp Med 2018;215:1803-1812.
7. Yokoi T, Murakami M, Kihara T, et al. Identification of a unique subset of tissue-resident memory CD4(+) T cells in Crohn's disease. Proc Natl Acad Sci U S A 2023;120:e2204269120.
8. Bishu S, El Zaatari M, Hayashi A, et al. CD4+ Tissue-resident Memory T Cells Expand and Are a Major Source of Mucosal Tumour Necrosis Factor α in Active Crohn's Disease. J Crohns Colitis 2019;13:905-915.
9. Thompson EA, Mitchell JS, Beura LK, et al. Interstitial migration of CD8αβ T cells in the small intestine is dynamic and is dictated by environmental cues. Cell reports 2019;26:2859-2867. e2854.
10. Chen B, Ye B, Li M, et al. TIGIT Deficiency Protects Mice From DSS-Induced Colitis by Regulating IL-17A-Producing CD4(+) Tissue-Resident Memory T Cells. Front Immunol 2022;13:931761.
11. Zheng GX, Terry JM, Belgrader P, et al. Massively parallel digital transcriptional profiling of single cells. Nature communications 2017;8:14049.
12. McGinnis CS, Murrow LM, Gartner ZJ. DoubletFinder: doublet detection in single-cell RNA sequencing data using artificial nearest neighbors. Cell systems 2019;8:329-337. e324.
13. Hao Y, Hao S, Andersen-Nissen E, et al. Integrated analysis of multimodal single-cell data. Cell 2021;184:3573-3587. e3529.
14. Finak G, McDavid A, Yajima M, et al. MAST: a flexible statistical framework for assessing transcriptional changes and characterizing heterogeneity in single-cell RNA sequencing data. Genome biology 2015;16:1-13.
15. Wu T, Hu E, Xu S, et al. clusterProfiler 4.0: A universal enrichment tool for interpreting omics data. The innovation 2021;2
16. Korotkevich G, Sukhov V, Budin N, et al. Fast gene set enrichment analysis. BioRxiv 2016:060012.
17. Aibar S, González-Blas CB, Moerman T, et al. SCENIC: single-cell regulatory network inference and clustering. Nature methods 2017;14:1083-1086.
18. Huynh-Thu VA, Irrthum A, Wehenkel L, et al. Inferring regulatory networks from expression data using tree-based methods. PloS one 2010;5:e12776.

19. Zhang L, Yu X, Zheng L, et al. Lineage tracking reveals dynamic relationships of T cells in colorectal cancer. Nature 2018;564:268-272.
20. Nazarov VI, Pogorelyy MV, Komech EA, et al. tcR: an R package for T cell receptor repertoire advanced data analysis. BMC bioinformatics 2015;16:1-5.
21. Browaeys R, Saelens W, Saeys Y. NicheNet: modeling intercellular communication by linking ligands to target genes. Nature methods 2020;17:159-162.
22. Beura LK, Fares-Frederickson NJ, Steinert EM, et al. CD4+ resident memory T cells dominate immunosurveillance and orchestrate local recall responses. Journal of Experimental Medicine 2019;216:1214-1229.
23. Romagnoli P, Fu H, Qiu Z, et al. Differentiation of distinct long-lived memory CD4 T cells in intestinal tissues after oral Listeria monocytogenes infection. Mucosal immunology 2017;10:520-530.
24. Sathaliyawala T, Kubota M, Yudanin N, et al. Distribution and compartmentalization of human circulating and tissue-resident memory T cell subsets. Immunity 2013;38:187-197.
25. Chang C, Loo C-S, Zhao X, et al. The nuclear receptor REV-ERBα modulates Th17 cell-mediated autoimmune disease. Proceedings of the National Academy of Sciences 2019;116:18528-18536.
26. Ivanov II, McKenzie BS, Zhou L, et al. The orphan nuclear receptor RORγt directs the differentiation program of proinflammatory IL-17+ T helper cells. Cell 2006;126:1121-1133.
27. Vesely MCA, Pallis P, Bielecki P, et al. Effector TH17 cells give rise to long-lived TRM cells that are essential for an immediate response against bacterial infection. Cell 2019;178:1176-1188. e1115.
28. Wang C, Kang SG, Lee J, et al. The roles of CCR6 in migration of Th17 cells and regulation of effector T-cell balance in the gut. Mucosal immunology 2009;2:173-183.
29. Ciofani M, Madar A, Galan C, et al. A validated regulatory network for Th17 cell specification. Cell 2012;151:289-303.
30. Glanville J, Huang H, Nau A, et al. Identifying specificity groups in the T cell receptor repertoire. Nature 2017;547:94-98.
31. Robertson G, Hirst M, Bainbridge M, et al. Genome-wide profiles of STAT1 DNA association using chromatin immunoprecipitation and massively parallel sequencing. Nat Methods 2007;4:651-657.
32. Kano S, Sato K, Morishita Y, et al. The contribution of transcription factor IRF1 to the interferon-gamma-interleukin 12 signaling axis and TH1 versus TH-17 differentiation of CD4+ T cells. Nat Immunol 2008;9:34-41.
33. Matos TR, O'Malley JT, Lowry EL, et al. Clinically resolved psoriatic lesions contain psoriasis-specific IL-17-producing αβ T cell clones. J Clin Invest 2017;127:4031-4041.
34. Gallais Sérézal I, Classon C, Cheuk S, et al. Resident T Cells in Resolved Psoriasis Steer Tissue Responses that Stratify Clinical Outcome. J Invest Dermatol 2018;138:1754-1763.
35. Basdeo SA, Cluxton D, Sulaimani J, et al. Ex-Th17 (Nonclassical Th1) Cells Are Functionally Distinct from Classical Th1 and Th17 Cells and Are Not Constrained by Regulatory T Cells. J Immunol 2017;198:2249-2259.
36. Neurath MF. New targets for mucosal healing and therapy in inflammatory bowel diseases. Mucosal Immunol 2014;7:6-19.
37. Hueber W, Sands BE, Lewitzky S, et al. Secukinumab, a human anti-IL-17A monoclonal antibody, for

moderate to severe Crohn's disease: unexpected results of a randomised, double-blind placebo-controlled trial. Gut 2012;61:1693-1700.

38. Blanco FJ, Möricke R, Dokoupilova E, et al. Secukinumab in Active Rheumatoid Arthritis: A Phase III Randomized, Double-Blind, Active Comparator- and Placebo-Controlled Study. Arthritis Rheumatol 2017;69:1144-1153.
39. Mills KHG. IL-17 and IL-17-producing cells in protection versus pathology. Nat Rev Immunol 2023;23:38-54.
40. Hirota K, Duarte JH, Veldhoen M, et al. Fate mapping of IL-17-producing T cells in inflammatory responses. Nat Immunol 2011;12:255-263.
41. Puel A, Cypowyj S, Bustamante J, et al. Chronic mucocutaneous candidiasis in humans with inborn errors of interleukin-17 immunity. Science 2011;332:65-68.
42. Chong WP, Mattapallil MJ, Raychaudhuri K, et al. The Cytokine IL-17A Limits Th17 Pathogenicity via a Negative Feedback Loop Driven by Autocrine Induction of IL-24. Immunity 2020;53:384-397.e385.
43. Lee JS, Tato CM, Joyce-Shaikh B, et al. Interleukin-23-Independent IL-17 Production Regulates Intestinal Epithelial Permeability. Immunity 2015;43:727-738.
44. Maxwell JR, Zhang Y, Brown WA, et al. Differential Roles for Interleukin-23 and Interleukin-17 in Intestinal Immunoregulation. Immunity 2015;43:739-750.
45. Zielinski CE, Mele F, Aschenbrenner D, et al. Pathogen-induced human TH17 cells produce IFN-γ or IL-10 and are regulated by IL-1β. Nature 2012;484:514-518.
46. Kiner E, Willie E, Vijaykumar B, et al. Gut CD4(+) T cell phenotypes are a continuum molded by microbes, not by T(H) archetypes. Nat Immunol 2021;22:216-228.
47. Lee HS, Vancamelbeke M, Verstockt S, et al. Molecular Changes in the Non-Inflamed Terminal Ileum of Patients with Ulcerative Colitis. Cells 2020;9
48. Smillie CS, Biton M, Ordovas-Montanes J, et al. Intra- and Inter-cellular Rewiring of the Human Colon during Ulcerative Colitis. Cell 2019;178:714-730.e722.

국문요약

크론병은 위장장벽을 침범하는 만성 염증성 질환이다. 조직 상주 기억 T 세포는 크론병과 관련된 것으로 알려졌지만, 그 특성은 아직 불분명하다. 본 연구는 단일 세포 전사체를 통해서 크론병 환자의 소장 내에 존재하는 조직 상주 기억 T 세포의 기능적 특성 및 면역 세포와의 상호작용을 조사하는 것을 목표로 했다. 크론병 환자 7명과 궤양성대장염 환자 4명의 소장 조직이 분석에 사용되었으며, 궤양성대장염 환자의 소장 조직은 대조군으로써 사용되었다. 각 환자의 소장 조직을 고유판 분획과 점막하층/근육층 분획으로 분리한 후, 단일 세포 전사체 분석과 T 세포 수용체 분석을 수행했다. T 세포 58,123개를 Th17 조직 상주 기억 T 세포, $CD4^+$ 조직 상주 기억 T 세포 및 $CD8^+$ 조직 상주 기억 T 세포 집단을 포함한 16개의 집단으로 그룹화하였다. 이중 Th17 조직 상주 기억 T 세포 집단은 *IL17A*, *IL22* 및 *CCL20*과 같은 Th17 특성 관련 유전자들과 함께, *ITGAE*, *ITGA1* 및 *CXCR6*와 같은 조직 상주 마커 유전자들의 높은 발현을 보였다. 크론병 환자의 경우 대조군에 비해 고유판과 점막하층/근육층 영역 모두에서 Th17 조직 상주 기억 T 세포의 비율이 유의하게 증가했다. 또한 Th17 조직 상주 기억 T 세포 집단은 다른 $CD4^+$ T 세포 집단보다 높은 클론 확장을 보였다. 크론병 환자와 대조군 간의 Th17 조직 상주 기억 T 세포 차등 발현 유전자 분석 결과, 크론병 환자에서 IFNγ의 생성과 관련된 유전자들의 발현이 유의하게 증가하였다. 크론병 환자의 Th17 조직 상주 기억 T 세포에서 발현이 증가한 IFNγ는 골수성 세포에서 다양한 케모카인들의 발현 증가를 유도하는 것으로 예측되었다. 본 연구는 크론병 환자의 소장 전체에 걸쳐 Th17 조직 상주 기억 T 세포의 증가를 확인했으며, 이는 IFNγ의 유도 및 골수성 세포에서의 케모카인 생성을 통해 질병 발병에 기여할 가능성을 시사한다.